*nanomaterials*

MDPI

*Article*

# Large-Scale $MoS_2$ Pixel Array for Imaging Sensor

**Kang Liu [1,†], Xinyu Wang [1,†], Hesheng Su [1], Xinyu Chen [1], Die Wang [1], Jing Guo [1], Lei Shao [2,*], Wenzhong Bao [1,*] and Honglei Chen [3,*]**

[1] State Key Laboratory of ASIC and System, School of Microelectronics, Zhangjiang Fudan International Innovation Center, Fudan University, Shanghai 200433, China
[2] School of Electronic Information, Soochow University, Suzhou 215006, China
[3] Shanghai Institute of Technical Physics, Chinese Academy of Sciences, Shanghai 200083, China
* Correspondence: shaolei@suda.edu.cn (L.S.); baowz@fudan.edu.cn (W.B.); chenhl@mail.sitp.ac.cn (H.C.)
† These authors contributed equally to this work.

**Abstract:** Two-dimensional molybdenum disulfide ($MoS_2$) has been extensively investigated in the field of optoelectronic devices. However, most reported $MoS_2$ phototransistors are fabricated using the mechanical exfoliation method to obtain micro-scale $MoS_2$ flakes, which is laboratory- feasible but not practical for the future industrial fabrication of large-scale pixel arrays. Recently, wafer-scale $MoS_2$ growth has been rapidly developed, but few results of uniform large-scale photoelectric devices were reported. Here, we designed a 12 × 12 pixels pixel array image sensor fabricated on a 2 cm × 2 cm monolayer $MoS_2$ film grown by chemical vapor deposition (CVD). The photogating effect induced by the formation of trap states ensures a high photoresponsivity of 364 $AW^{-1}$, which is considerably superior to traditional CMOS sensors (≈0.1 $AW^{-1}$). Experimental results also show highly uniform photoelectric properties in this array. Finally, the concatenated image obtained by laser lighting stencil and photolithography mask demonstrates the promising potential of 2D $MoS_2$ for future optoelectrical applications.

**Keywords:** molybdenum disulfide ($MoS_2$); two-dimensional (2D) semiconductors; photo sensor



**Citation:** Liu, K.; Wang, X.; Su, H.; Chen, X.; Wang, D.; Guo, J.; Shao, L.; Bao, W.; Chen, H. Large-Scale $MoS_2$ Pixel Array for Imaging Sensor. *Nanomaterials* **2022**, *12*, 4118. https://doi.org/10.3390/nano12234118

Academic Editor: Antonio Di Bartolomeo

Received: 28 October 2022
Accepted: 18 November 2022
Published: 22 November 2022



## 1. Introduction

Two-dimensional (2D) transition metal dichalcogenides (TMDs) have been developing rapidly and have received considerable research attention in the field of photodetection because of their superior electrical and optical properties [1–4]. Tremendous efforts have been dedicated to developing high-performance 2D TMDs-based photodetectors for potential applications in optical imaging, neural network vision sensor, and bioinspired in-sensor vision [5–9]. Molybdenum disulfide ($MoS_2$), the most famous representative in the TMD family, has been extensively investigated for electronic and optoelectronic device applications owing to its unique properties, including the layer-dependent bandgap (1.8~1.2 eV from monolayer to bulk), relatively high electron mobility, and current on/off ratio (up to $10^9$) [10–13]. Therefore, $MoS_2$ has been considered a promising channel material for low-power logic devices [14–16] and photodetectors in the visible range [17]. Most previously reported results were based on isolated $MoS_2$ flakes obtained via widely-used top-down approaches such as mechanical exfoliation [18,19]. Such exfoliated single crystalline flakes provide good performance for a single fabricated device, but their micro-scale flake sizes and randomly distributed thicknesses also result in low yield and reproducibility, which hinder practical device applications [18,20].

In recent years, the large-scale fabrication of $MoS_2$ devices has become mainstream since various wafer-scale bottom-up growth methods have been developed, such as CVD, atomic layer deposition (ALD), and metal-organic CVD (MOCVD). For example, Peng et al. presented CVD-grown $MoS_2$ phototransistors with a high photoresponsivity of 6650 $AW^{-1}$ and detectivity of 1.23 × $10^{12}$ [21]. Chu et al. produced a molybdenum-based phototransistor with an ultrasensitive detectivity of 9.8 × $10^{16}$ cm $Hz^{1/2}$ $W^{-1}$ [22]. Guo et al.

reported the optoelectrical performances of stacked ML-$MoS_2$ phototransistors [23]. In addition to the film fabrication, various device structures have been proposed to improve the performance of $MoS_2$ photodetectors. Chen et al. presented a bilayer $MoS_2$/graphene heterostructure array with the photoresponsivity of 32 $mAW^{-1}$ [24]. Jeong et al. demonstrated a periodically arrayed nanopore structures for improving the efficiency of multilayered p-$WSe_2$/n-$MoS_2$ phototransistors with a photoresponsivity of $1.7 \times 10^4$ $AW^{-1}$ [25]. However, none of the above focused on the homogeneity of large-scale 2D TMD photodetector arrays, which is a key to realize a practical image sensor. Recently, several reported results tackled the fabrication of pixel array $MoS_2$ image sensors. Park et al. reported a $4 \times 4$ multilayer $MoS_2$ phototransistors array grown using a post-sulfurization process, which gives rise to a high uniformity but at the cost of a relatively low photoresponsivity of 3.7 $AW^{-1}$ [26]. Hong et al. designed an $8 \times 8$ active pixel image sensor array based on a bilayer $MoS_2$ film with a maximum photoresponsivity of 119.16 $AW^{-1}$ [27]. In these works, how to maintain a uniform high performance while increasing the scale of the pixel array still remains an unsolved problem. In this study, we presented a $12 \times 12$ pixel array image sensor built on a 2 cm $\times$ 2 cm monolayer $MoS_2$ film. Compared with previous work, all 144 individual pixels exhibit the desired optoelectrical properties (photoresponsivity of 364 $AW^{-1}$, photo detectivity of $2.13 \times 10^{10}$) with a high uniformity. Moreover, the $MoS_2$ image sensor, placed under photolithography masks, was exposed to lights of visible-band wavelengths from a laser emitter. By illumination with a different wavelength and different stencils, three sets of photocurrent data were collected and converted to a visualization image, respectively. Thus, this work introduces a new platform for optoelectronic application of wafer-scale 2D-TMDs such as ultra-thin image sensors, transparent image sensors, artificial intelligence photo sensors, and selective light-detecting imagers.

## 2. Materials Synthesis and Characterizations

Our pixel array image sensor was formed using a 2 cm $\times$ 2 cm CVD-grown monolayer $MoS_2$ film, as shown in Figure 1a. This film was synthesized directly on a cleaned silicon oxide ($SiO_2$) substrate without any transfer processes [28]. Compared with the transferring method, the CVD growing method does not use complex processes, implying a higher productivity and lower cost. More details on the film growth are provided in the Supplementary Materials. Prior to the device fabrication, multiple material characteristics, Raman spectra, photoluminescence (PL) spectra, atomic transmission microscope (AFM), and SHG were tested, and the corresponding results were given in Figure 1. In Figure 1b, the Raman spectra under the irradiation of a 514 nm laser were obtained from five different locations on the $MoS_2$ film. The difference between two dominant peaks, i.e., the in-plane ($E^1{}_{2g}$) vibration mode at ~384.3 $cm^{-1}$ and the out-of-plane ($A_{1g}$) vibration mode at ~404.7 $cm^{-1}$ was around 20 $cm^{-1}$, which was consistent with previous work [18]. Moreover, the prominent consistency and nonexistence of splitting of all Raman spectra curves indicated the high uniformity of our CVD-grown $MoS_2$ film. Figure 1c demonstrated the PL spectra from five suspended samples excited with a solid-state laser at a wavelength of 514 nm. A low laser power of 50 μW (on the sample) was used to avoid heating and PL saturation. The peak value at ≈1.84 eV in the PL spectra was a signal from the $MoS_2$ with silicon substrate [28]. Furthermore, the near-identical peak positions of all curves validated the wafer-scale uniformity of the film as well. The height profile of $MoS_2$ film was measured by AFM (Bruker Dimension Edge). The average height difference along the red line, as shown in Figure 1e, was around 0.78 nm, which corresponded exactly to the thickness of monolayer $MoS_2$ film [11]. Since the information on domain size and boundaries was missing through AFM, a second harmonic generation (SHG) technique was applied to reveal more detailed morphology. As shown in Figure 1f, the domain size was about 10–20 μm in our monolayer, $MoS_2$ and the grain boundaries could be clearly recognized from SHG images. Such capability of direct visualization of the grain information in $MoS_2$ is attributed to the suppressed SHG signal at the grain boundaries. The difference in crystal orientations resulted in the destructive interference and annihilation of the nonlinear

waves [29,30]. Above all, all the measurement results indicated the excellent uniformity of our CVD-grown film, which is crucial for further $MoS_2$ phototransistor device fabrication.

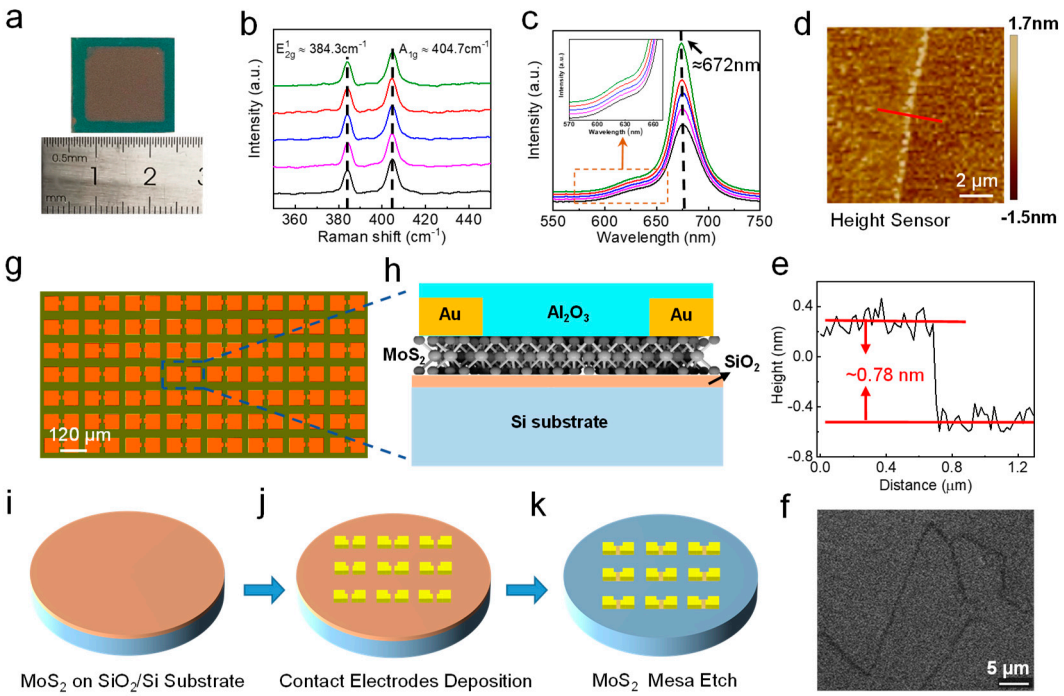


**Figure 1.** Spectroscopic analysis of the CVD-grown monolayer $MoS_2$ film and process of the device structure. (**a**) Photograph of an as-fabricated centimeter scale $MoS_2$ with FETs. (**b**) Raman spectra curves of five randomly selected points from the film, (**c**) PL spectra curves of five points with the same positions from the film, (**e**) thickness scan along the red line across the boundary of the film. (**d**) AFM image of the monolayer $MoS_2$ film. (**f**) SHG mapping in an area of 30 μm × 30 μm of the film, scale bar: 5 μm. (**g**) Optical microscopy image of the as-fabricated 12 × 12 $MoS_2$ phototransistors array. The scale bar is 120 μm. (**h**) 3D schematic image of a single $MoS_2$-based phototransistor. (**i**–**k**) diagram for the fabrication process of $MoS_2$ film to phototransistors devices employing back metal gates device structure.

The mature back-gate phototransistor structure was adopted here, and the detailed process is presented in Figure 1. The optical microscopic image of the pixel array photodetector with a large-area monolayer $MoS_2$ film is demonstrated in Figure 1g. The device was composed of 12 × 12 $MoS_2$ phototransistors with the same geometric size. A more detailed single device structure was illustrated in Figure 1h. Each phototransistor consists of a $MoS_2$ channel with W/L of 30 μm/20 μm and Au electrodes for source and drain contacts. Figure 1i–k displays a schematic fabrication flow of our $MoS_2$ pixelarray image sensor. As described before, the monolayer $MoS_2$ film was grown on a $SiO_2$/Si substrate, Au (35 nm), as the source/drain (S/D) electrodes were deposited using an electron-beam evaporator and photolithography via a lift-off technique, and then the channel isolation was realized by the $CF_4$ reactive ion etching using a photoresist mask, and a $MoS_2$ channel was etched to the designated dimensions. Finally, Aluminum oxide (40 nm) was deposited as the protective insulator via ALD. The details of the device fabrication are presented in the Supplementary Information.

Compared with the top-gate phototransistor structure, the back gate structured phototransistor can absorb light more efficiently. Moreover, $MoS_2$ is directly grown on a $SiO_2$/Si substrate without additional processing (e.g., transferring $MoS_2$ onto a glass or flexible substrate [31]), which also contributes to a higher uniformity and lower fabrication cost.

## 3. Results and Discussion

Then, we tested the electrical properties of as-fabricated $MoS_2$ phototransistors. The typical transfer characteristics ($I_D$-$V_{BG}$) of a single $MoS_2$ phototransistor was plotted in Figure 2a. The current on/off ratio ($I_{on}/I_{off}$) of ≈$10^6$ and the threshold voltage ($V_{TH}$) of −9.2 V at a drain voltage ($V_{DS}$) of 1 V indicated the strong gate modulation of the designed $MoS_2$ device. Figure 2b displayed the output characteristics of a typical $MoS_2$ phototransistor in the pixel array image sensor. The drain current ($I_D$) was saturated at a high drain bias (>20 V) because of pinch-off at the drain region. Due to a satisfied contact formation between the monolayer $MoS_2$ film and the S/D electrodes (Au), the output characteristics, $I_D$-$V_{DS}$, in the insets of Figure 2b exhibited a linear behavior of $I_D$ at a low drain bias [32]. Field-effect carrier mobility $\mu_{eff}$ could also be extracted from the linear region of the transfer curve using the following equation $\mu_{eff} = g_m \frac{L_c}{W_c C_{ox} V_{DS}}$, where $g_m$ is the transconductance, $L_c$ and $W_c$ are the length and width of the channel, respectively, $C_{ox}$ is the capacitance of the gate insulator, and $V_{DS}$ is the drain voltage [33].

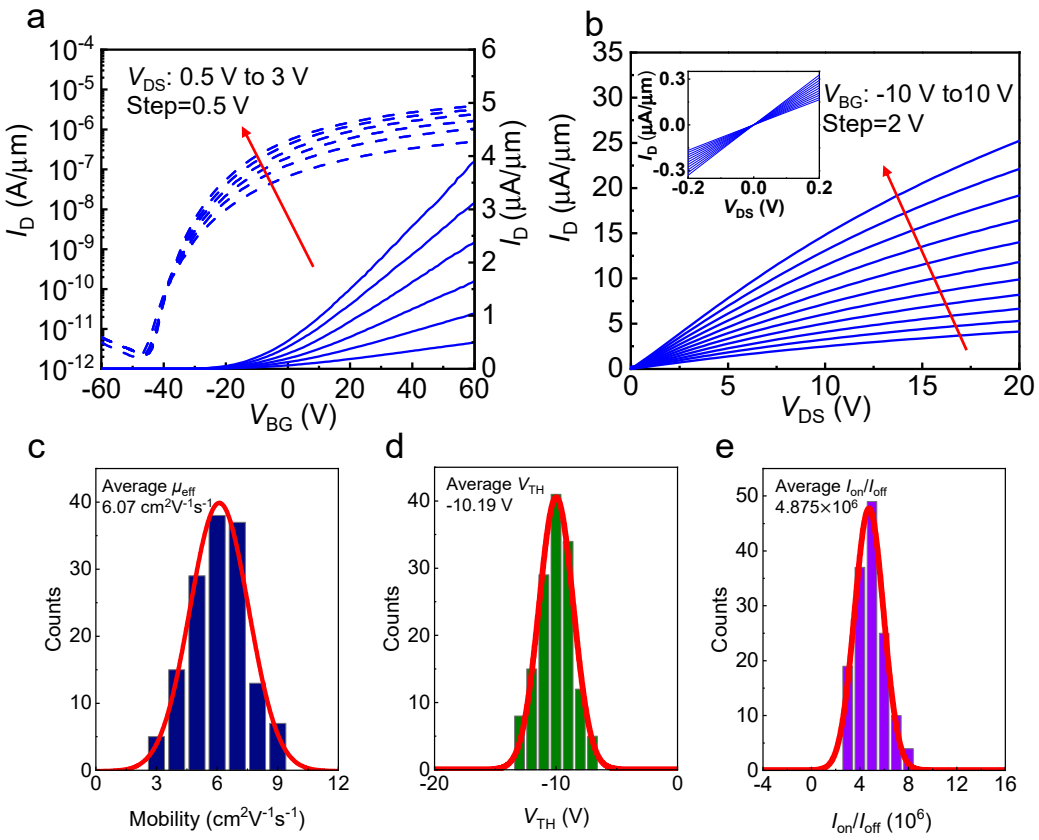


**Figure 2.** Electrical characteristics and statistical analysis of $MoS_2$ phototransistors. (**a**) $I_D$-$V_{BG}$ curves of a typical $MoS_2$ phototransistor at $V_{DS}$ from 0.5 to 3 V with the step of 0.5 V. (**b**) $I_D$-$V_{DS}$ curves of $MoS_2$ at $V_{BG}$ from −10 to 10 V with the step of 2 V. Inset: $I_D$-$V_{DS}$ curve acquired at a small range of $V_{DS}$. The Histograms of (**c**) field-effect mobility (average $\mu_{eff}$ = 6.07 cm$^2$ V$^{-1}$ s$^{-1}$), (**d**) threshold voltage (average $V_{TH}$ = −10.19 V), and (**e**) $I_{on}/I_{off}$ current ratio (average $I_{on}/I_{off}$ = 4.875 × $10^6$) with $V_{DS}$ = 1 V of all 12 × 12 $MoS_2$ phototransistor pixels.

To further demonstrate the uniformity of our image sensor in terms of electrical properties, histogram and corresponding fitted Gaussian distribution were also calculated for mobility ($\mu_{eff}$), threshold voltage ($V_{TH}$), and on/off current ratio ($I_{on}/I_{off}$) measured from all 12 × 12 phototransistors, as summarized in Figure 2c–e, respectively. The corresponding fitted Gaussian curves (the red solid lines) were also plotted for each parameter. All the phototransistors exhibited a satisfactory electrical performance with the following average values: a $\mu_{eff}$ of 6.07 cm$^2$ V$^{-1}$ s$^{-1}$, a $V_{TH}$ of −10.2 V, and an $I_{on}/I_{off}$ of 4.87 × $10^6$. According

the equation $STD(D) = \sqrt{\frac{\sum_{i=1}^{144}(D_i - \overline{D})^2}{144}}/\overline{D}$, where $D$ could be replaced by $\mu_{\text{eff}}$, $V_{\text{TH}}$ and $I_{\text{on}}/I_{\text{off}}$. The standard deviations ($STD$) of carrier mobility $\mu_{\text{eff}}$ is 23%. The $STD$ of threshold voltage $V_{\text{TH}}$ and current ratio $I_{\text{on}}/I_{\text{off}}$ are 2.8% and 25.2%, respectively. Compared with previous works [26,27], our image sensor exhibited better electrical performance and much smaller pixel-level variation with a much greater number of phototransistors.

In addition to the electrical characteristics, the key opto-electric characteristics of a single $MoS_2$ phototransistor were measured in Figure 3. Figure 3a exhibited the photoinduced transfer characteristics $I_D$-$V_{BG}$ for a typical $MoS_2$ photodetector 550 nm illumination wavelength at given incident power densities ($P_{\text{in}}$) ranging from 14.7 to 285.9 μW/cm$^2$. The photocurrent curve of Figure 3b was further extracted from Figure 3a by the following equation: $I_{\text{PH}} = I_{\text{illumination}} - I_{\text{dark}}$. The photocurrent of the monolayer $MoS_2$ phototransistor gradually increased with increasing $P_{\text{in}}$ according to the photocurrent value under light with different power densities. Moreover, the photoinduced transfer characteristics and photocurrent curve under light with changeable excitation wavelength are presented in Figure 3d,e. Monolayer $MoS_2$ is more sensitive to visible wavelength band (420–680 nm) compared with near-infrared band (700–1200 nm). Figure 3c,f displayed the curve of the calculated photoresponsivity $R_{\text{PH}}$ as a function of incident power density and excitation wavelength, which were important figures of merit for phototransistors. The $R_{\text{PH}}$ was extracted from the transfer characteristics in Figure 3b,e using the equation of $R_{\text{PH}} = I_{\text{PH}}/P_{\text{in}}$ (unit: AW$^{-1}$), where $I_{\text{PH}}$ and $P_{\text{in}}$ are the photocurrent and incident power density, respectively. The main mechanism for the high $R_{\text{PH}}$ of the monolayer $MoS_2$ phototransistor is the photogating (PG) effect by the formation of trap states near the valance band due to the structural imperfection and defects of $MoS_2$ [34–37].

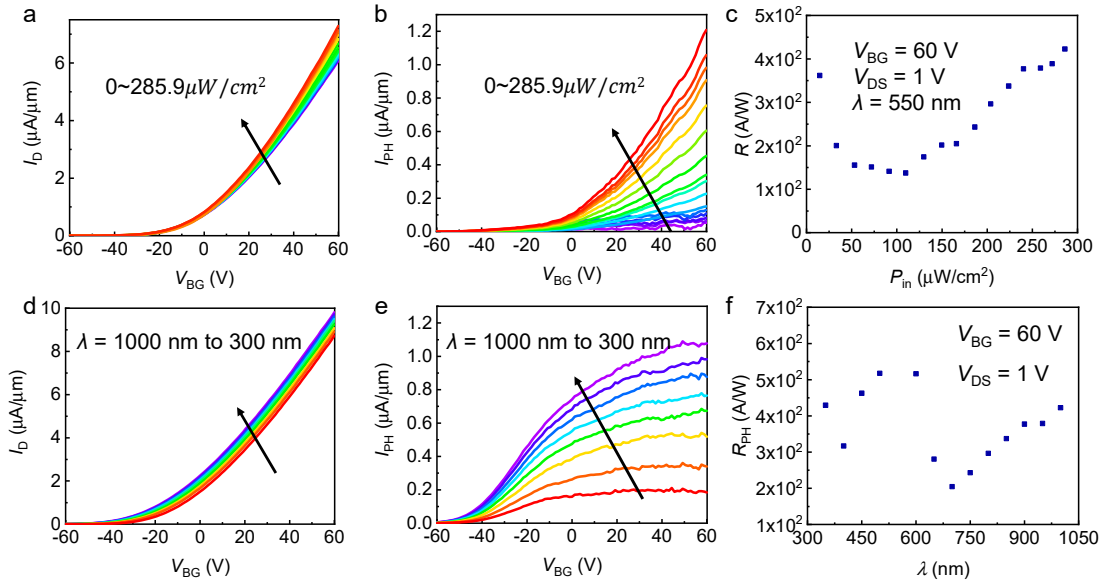


**Figure 3.** Photo-responsive characteristics of a monolayer $MoS_2$ phototransistor in the image sensor array. (**a**) Transfer curves of $I_D$ for dark and illumination conditions and (**b**) Photocurrent as the function of $V_{BG}$ when $V_{DS}$ = 1 V with varying lighting intensity, ranging from 14.7 to 285.9 μW/cm$^2$ with an average step of 17.87 μW/cm$^2$. (**c**) Responsivity as a function of incident power when $V_{BG}$ = 60 V and $V_{DS}$ = 1 V. (**d**) Transfer curves for illumination conditions with varying light wavelengths. (**e**) Photocurrent as a function of $V_{BG}$ when $V_{DS}$ = 1 V with different wavelengths, ranging from 1000 nm to 300 nm with a step of −100 nm. (**f**) Responsivity as a function of the light wavelength.

Finally, Figure 4 presents the photo-response speed and an overall uniformity of the 12 × 12 $MoS_2$ array. Figure 4a showed its switching behaviors under pulsed RGB light illumination. As it can be noticed, the photoresponsivity under 450 nm laser was much larger but with a slower response than that of the 750 nm laser. The rise time and decay time

increased as light wavelength decreases due to a more excited number of photogenerated charge carriers [36,38]. Figure 4b showed a light intensity dependence, in which the $I_{PH}$ and response time are all positively correlated to incident power, which is also attributed to the photogating effect [17]. Figure 4c presents the photo-switching behavior of $I_{PH}$ under different $V_{DS}$ values. The photoresponsivity increases at the expense of a longer response time. The switching characteristics under different back-gate voltages ($V_{BG}$) are displayed in Figure S1. When $V_{BG}$ was over-high (>10 V) or over-low (<−10 V), the recovery time would be longer for photo-excited carriers to detrap from the subgap state [27], whereas the gate pulse method by changing back-gate voltage $V_{BG}$ would improve greatly the response speed of our image sensor array. As shown in Figure 4d, when the illumination switched from light to dark, the $V_{BG}$ was injected simultaneously with a short-time (≈1 s) pulse voltage from 8 V to 15 V to suppress carriers as soon as possible. As a result, the falling time decreased by 90% compared with Figure 4a–c. A more detailed gate pulse effect was displayed in Figure S2 and Table S1. A short duration gate voltage pulse could reduce the decay time significantly due to the detrapping of the trapped holes in subgap states, which enables the high-speed operation of the $MoS_2$ image sensor [27,39].

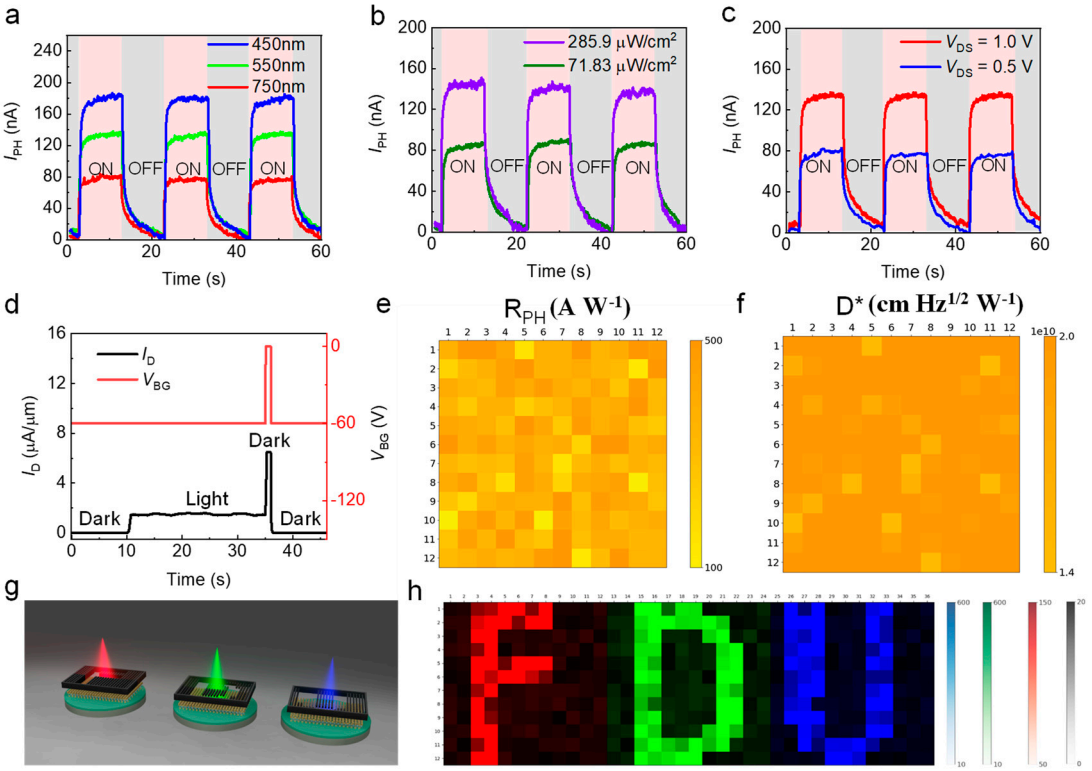


**Figure 4.** (**a**) Time-trace of the photodetector under illumination with the same intensity ($P_{in}$ = 200 μW/cm$^2$) and $V_{DS}$ = 1 V but at different wavelengths ($\lambda$ = 450, 550 and 750 nm). (**b**) Same measure for different light intensities ($P_{in}$ = 285.9 μW/cm$^2$ and 71.83 μW/cm$^2$) with the wavelength of 550 nm and $V_{DS}$ = 1 V. (**c**) Same measurement for different $V_{DS}$ values (0.5 and 1.0 V) under the illumination of 285.9 μW/cm$^2$ with 550 nm wavelength. (**d**) Photo-switching characteristics with gate pulse. (**e**,**f**) Photo-responsivity and detectivity mapping of 144 $MoS_2$ phototransistors under the illumination of 285.9 μW/cm$^2$ with 550 nm wavelength. (**g**) Measurement concept using the light stencil projection for image detection of the image sensor array. The 12 × 12 monolayer $MoS_2$ image sensor array is placed behind character masks and measured photoelectricity under RGB light illumination (wavelength $\lambda$ = 750, 550, and 450 nm). (**h**) Horizontal concatenated normalized image with a resolution of 36 × 12 pixels.

To demonstrate the overall uniformity of our image sensor, a statistical distribution of the photoelectrical properties, i.e., responsivity and detectivity of 12 × 12 $MoS_2$ phototransistors was confirmed in the mapping images that presented the current level of each phototransistor under illumination with $P_{in}$ of 285.9 μW/cm$^2$ (Figure 4e,f), respectively, where all currents were measured at a $V_{DS}$ of 1 V. The detectivity ($D^*$) is obtained by the equation of $D^* = \sqrt{\frac{A}{2qI_D}}R_{PH}$, where $A$ is the channel area, $q$ is unit electric charge, $I_D$ is dark current, and $R_{PH}$ is photoresponsivity. The average photoresponsivity was 364.00 AW$^{-1}$ with a standard deviation of 99 AW$^{-1}$. The detectivity was 2.16 × 10$^{10}$ cm Hz$^{1/2}$ W$^{-1}$ with a standard deviation of 3.23 × 10$^9$ cm Hz$^{1/2}$ W$^{-1}$. The photocurrent maps under illumination with different wavelengths (red: 750 nm, green: 550 nm, blue: 450 nm) are demonstrated in Figure S3, which also proves the uniformity of our device.

Moreover, three sets of masks (each was 12 × 12 pixels) with different characters ("F", "D" and "U") were prepared and patterned using a laser cutting system, as shown in Figure 4g, to evaluate the image-sensing characteristics of the monolayer $MoS_2$ image sensor array. These character masks were sequentially placed on the image sensor array during light projection (red: 750 nm, green: 550 nm, blue: 450 nm). The 2D photocurrent data, collected under light stencil, was firstly normalized from float type to then concatenated horizontally to form the final 36 × 12 image (total pixel: 576). Due to the uniform photo-related properties of all 12 × 12 phototransistors, the photosensitivity mapping result could display three characters clearly. Table 1 compared the fundamental properties with former works.

**Table 1.** Comparison of photo-related properties of fabricated pixel array image sensors.

| Indicator | Park et al. [26] | Hong et al. [27] | Ours |
|---|---|---|---|
| Pixel size (width × height) | 4 × 4 | 8 × 8 | 12 × 12 |
| Layer of $MoS_2$ film | 2 L | Multilayer | 1 L |
| Average responsivity (Unit: A W$^{-1}$) | 0.503 | 119.16 | 364.00 |
| Std responsivity (Unit: percentage %) | 15 | – | 27.2 |
| Average detectivity (Unit: cm Hz$^{1/2}$ W$^{-1}$) | 1.4 × 10$^4$ | 4.66 × 10$^6$ | 2.13 × 10$^{10}$ |
| Std detectivity (Unit: percentage %) | 12 | – | 15 |

## 4. Conclusions

In this paper, a 12 × 12 phototransistor pixel array image sensor based on a wafer-scale monolayer $MoS_2$ film was fabricated to present the potential of the next generation photodetector. The integrated pixel number is significantly increased without sacrificing photodetector performance. The fabricated $MoS_2$ devices showed high uniformity in electrical properties, including carrier mobility (≈6.07 cm$^2$ V$^{-1}$ s$^{-1}$), $I_{on}/I_{off}$ (≈4.875 × 10$^6$), and threshold voltage $V_{TH}$ (≈−10.19 V). The measured photoresponsivity $R_{PH}$ (≈364 AW$^{-1}$) and detectivity (≈2.13 × 10$^{10}$) were superior to traditional CMOS image sensors [40,41], which were attributed to the predominant photogeneration mechanism of the PG effect induced by the formation of trap states near the valance band due to the structural imperfection and defects of $MoS_2$. These results provide a blueprint for the future development of wafer-scale 2D TMD optoelectrical application and suggest further application scenarios requiring a high dynamic range, such as with artificial retinas.

**Supplementary Materials:** The following supporting information can be downloaded at: https://www.mdpi.com/article/10.3390/nano12234118/s1, Figure S1: Photoswitching characteristics of the $MoS_2$ phototransistor under temporal light illumination with varying back gate voltage $V_{BG}$ from −30 V to 30 V with a step of 10 V. All switching curves were measured at $V_{DS}$ = 1 V with illumination frequency of 0.05 Hz; Figure S2: A Time resolved photoresponsive characteristics of the monolayer $MoS_2$ phototransistor under temporal light illumination with λ = 550 nm without and with gate voltage pulse. The fall time is improved from 7.59 s to 6.24 s; Figure S3: Photocurrent mapping of 12 × 12 $MoS_2$ phototransistors at $V_{DS}$ = 1 V, $V_{BG}$ = −10 V under RGB light illumination (λ = 750, 550, and 450 nm), indicating uniform photocurrent photoresponses; Table S1: The rise time and fall time with different case. Reference [42] was cited in supplementary materials.

**Author Contributions:** Conceptualization, data curation, software, K.L. and X.W.; formal analysis, K.L., X.W. and H.S.; resources, supervision, L.S., H.C. and W.B.; writing—review and editing, K.L., X.W., H.S., X.C., D.W. and J.G. All authors have read and agreed to the published version of the manuscript.

**Funding:** This research was funded by the National Key Research and Development Program (Grant No. 2021YFA1200500), in part by the Innovation Program of Shanghai Municipal Education Commission (Grant No. 2021-01-07-00-07-E00077), and Shanghai Municipal Science and Technology Commission (Grant No. 21DZ1100900). We also thank the support of the young scientist project from the MOE innovation platform.

**Data Availability Statement:** The data presented in this study are available on request from the corresponding author.

**Conflicts of Interest:** The authors declare no conflict of interest.

## References

1. Xu, X.; Pan, Y.; Liu, S.; Han, B. Seeded 2D epitaxy of large-area single-crystal films of the van der Waals semiconductor 2H $MoTe_2$. *Science* **2021**, *372*, 195–200. [CrossRef] [PubMed]
2. Michailow, W.; Spencer, P.; Almond, N.W.; Kindness, S.J.; Wallis, R.; Mitchell, T.A.; Degl'Innocenti, R.; Mikhailov, S.A.; Beere, H.E.; Ritchie, D.A. An in-plane photoelectric effect in two-dimensional electron systems for terahertz detection. *Sci. Adv.* **2022**, *8*, eabi8398. [CrossRef] [PubMed]
3. Wang, Q.H.; Kalantar-Zadeh, K.; Kis, A.; Coleman, J.N.; Strano, M.S. Electronics and optoelectronics of two-dimensional transition metal dichalcogenides. *Nat. Nanotechnol.* **2012**, *7*, 699–712. [CrossRef] [PubMed]
4. Xia, F.; Wang, H.; Xiao, D.; Dubey, M.; Ramasubramaniam, A. Two-dimensional material nanophotonics. *Nat. Photonics* **2014**, *8*, 899–907. [CrossRef]
5. Koppens, F.H.; Mueller, T.; Avouris, P.; Ferrari, A.C.; Vitiello, M.S.; Polini, M. Photodetectors based on graphene, other two-dimensional materials and hybrid systems. *Nat. Nanotechnol.* **2014**, *9*, 780–793. [CrossRef]
6. Mennel, L.; Symonowicz, J.; Wachter, S.; Polyushkin, D.K.; Molina-Mendoza, A.J.; Mueller, T. Ultrafast machine vision with 2D material neural network image sensors. *Nature* **2020**, *579*, 62–66. [CrossRef]
7. Liao, F.; Zhou, Z.; Kim, B.; Chen, J.; Wang, J.; Wan, T.; Zhou, Y.; Hoang, A.; Wang, C.; Kang, J.; et al. Bioinspired in-sensor visual adaptation for accurate perception. *Nat. Electron.* **2022**, *5*, 84–91. [CrossRef]
8. Yu, J.; Yang, X.; Gao, G.; Xiong, Y.; Wang, Y.; Han, J.; Chen, Y.; Zhang, H.; Sun, Q.; Wang, Z.L. Bioinspired mechano-photonic artificial synapse based on graphene/$MoS_2$ heterostructure. *Sci. Adv.* **2021**, *7*, eabd9117. [CrossRef]
9. Hu, Y.; Dai, M.; Feng, W.; Zhang, X.; Gao, F.; Zhang, S.; Tan, B.; Zhang, J.; Shuai, Y.; Fu, Y.; et al. Ultralow Power Optical Synapses Based on $MoS_2$ Layers by Indium-Induced Surface Charge Doping for Biomimetic Eyes. *Adv. Mater.* **2021**, *33*, 2104960. [CrossRef]
10. Liu, L.; Li, T.; Ma, L.; Li, W.; Gao, S.; Sun, W.; Dong, R.; Zou, X.; Fan, D.; Shao, L.; et al. Uniform nucleation and epitaxy of bilayer molybdenum disulfide on sapphire. *Nature* **2022**, *605*, 69–75. [CrossRef]
11. Radisavljevic, B.; Radenovic, A.; Brivio, J.; Giacometti, V.; Kis, A. Single-layer $MoS_2$ transistors. *Nat. Nanotechnol.* **2011**, *6*, 147–150. [CrossRef] [PubMed]
12. Yoon, Y.; Ganapathi, K.; Salahuddin, S. How good can monolayer $MoS_2$ transistors be? *Nano Lett.* **2011**, *11*, 3768–3773. [CrossRef] [PubMed]
13. Mak, K.F.; Lee, C.; Hone, J.; Shan, J.; Heinz, T.F. Atomically thin $MoS_2$: A new direct-gap semiconductor. *Phys. Rev. Lett.* **2010**, *105*, 136805. [CrossRef]
14. Dodda, A.; Trainor, N.; Redwing, J.M.; Das, S. All-in-one, bio-inspired, and low-power crypto engines for near-sensor security based on two-dimensional memtransistors. *Nat. Commun.* **2022**, *13*, 3587. [CrossRef] [PubMed]
15. Waltl, M.; Knobloch, T.; Tselios, K.; Filipovic, L.; Stampfer, B.; Hernandez, Y.; Waldhor, D.; Illarionov, Y.; Kaczer, B.; Grasser, T. Perspective of 2D Integrated Electronic Circuits: Scientific Pipe Dream or Disruptive Technology? *Adv. Mater.* **2022**, 2201082. [CrossRef]

16. Zhu, K.; Wen, C.; Aljarb, A.; Xue, F.; Xu, X.; Tung, V.; Zhang, X.; Alshareef, H.; Lanza, M. The development of integrated circuits based on two-dimensional materials. *Nat. Electron.* **2021**, *4*, 775–785. [CrossRef]
17. Long, M.; Wang, P.; Fang, H.; Hu, W. Progress, challenges, and opportunities for 2D material based photodetectors. *Adv. Funct. Mater.* **2019**, *29*, 1803807. [CrossRef]
18. Lee, C.; Yan, H.; Brus, L.; Heinz, T.; Hone, J.; Ryu, S. Anomalous lattice vibrations of single-and few-layer $MoS_2$. *ACS Nano* **2010**, *4*, 2695–2700. [CrossRef]
19. Ermolaev, G.A.; El-Sayed, M.A.; Yakubovsky, D.I.; Voronin, K.V.; Romanov, R.I.; Tatmyshevskiy, M.K.; Doroshina, N.V.; Nemtsov, A.B.; Voronov, A.A.; Novikov, S.M. Optical Constants and Structural Properties of Epitaxial $MoS_2$ Monolayers. *Nanomaterials* **2021**, *11*, 1411. [CrossRef]
20. Coleman, J.N.; Lotya, M.; O'Neill, A.; Bergin, S.D.; King, P.J.; Khan, U.; Young, K.; Gaucher, A.; De, S.; Smith, R.J. Two-dimensional nanosheets produced by liquid exfoliation of layered materials. *Science* **2011**, *331*, 568–571. [CrossRef]
21. Peng, M.; Xie, R.; Wang, Z.; Wang, P.; Wang, F.; Ge, H.; Wang, Y.; Zhong, F.; Wu, P.; Ye, J.; et al. Blackbody-sensitive room-temperature infrared photodetectors based on low-dimensional tellurium grown by chemical vapor deposition. *Sci. Adv.* **2021**, *7*, eabf7358. [CrossRef] [PubMed]
22. Feng, S.; Liu, C.; Zhu, Q.; Su, X.; Qian, W.; Sun, Y.; Wang, C.; Li, B.; Chen, M.; Chen, L. An ultrasensitive molybdenum-based double-heterojunction phototransistor. *Nat. Commun.* **2021**, *12*, 4094. [CrossRef] [PubMed]
23. Guo, X.; Chen, H.; Bian, J.; Liao, F.; Ma, J.; Zhang, S.; Zhang, X.; Zhu, J.; Luo, C.; Zhang, Z.; et al. Stacking monolayers at will: A scalable device optimization strategy for two-dimensional semiconductors. *Nano Res.* **2022**, *15*, 6620–6627. [CrossRef]
24. Chen, C.; Feng, Z.; Feng, Y.; Yue, Y.; Qin, C.; Zhang, D.; Feng, W. Large-scale synthesis of a uniform film of bilayer $MoS_2$ on graphene for 2D heterostructure phototransistors. *ACS Appl. Mater. Interfaces* **2016**, *8*, 19004–19011. [CrossRef]
25. Jeong, M.H.; Ra, H.S.; Lee, S.H.; Kwak, D.H.; Ahn, J.; Yun, W.S. Multilayer $WSe_2/MoS_2$ Heterojunction Phototransistors through Periodically Arrayed Nanopore Structures for Bandgap Engineering. *Adv. Mater.* **2022**, *34*, e2108412. [CrossRef]
26. Park, H.; Liu, N.; Kim, B.H.; Kwon, S.H.; Baek, S.; Kim, S.; Lee, H.; Yoon, Y.J.; Kim, S. Exceptionally uniform and scalable multilayer $MoS_2$ phototransistor array based on large-scale $MoS_2$ grown by RF sputtering, electron beam irradiation, and sulfurization. *ACS Appl. Mater. Interfaces* **2020**, *12*, 20645–20652. [CrossRef] [PubMed]
27. Hong, S.; Liu, N.; Kim, B.H.; Kwon, S.H.; Baek, S.; Kim, S.; Lee, H.K.; Yoon, Y.J.; Kim, S. Highly sensitive active pixel image sensor array driven by large-area bilayer $MoS_2$ transistor circuitry. *Nat. Commun.* **2021**, *12*, 3559. [CrossRef]
28. Xu, H.; Zhang, H.; Guo, Z.; Shan, Y.; Wu, S.; Wang, J. High-performance wafer-scale $MoS_2$ transistors toward practical application. *Small* **2018**, *14*, 1803465. [CrossRef]
29. Yin, X.; Ye, Z.; Chenet, D.A.; Ye, Y.; O'Brien, K.; Hone, J.C.; Zhang, X. Edge nonlinear optics on a $MoS_2$ atomic monolayer. *Science* **2014**, *344*, 488–490. [CrossRef]
30. Li, D.; Xiao, Z.; Mu, S.; Wang, F.; Liu, Y.; Song, J. A facile space-confined solid-phase sulfurization strategy for growth of high-quality ultrathin molybdenum disulfide single crystals. *Nano Lett.* **2018**, *18*, 2021–2032. [CrossRef]
31. Choi, M.; Bae, S.R.; Hu, L.; Hoang, A.T.; Kim, S.Y.; Ahn, J.H. Full-color active-matrix organic light-emitting diode display on human skin based on a large-area $MoS_2$ backplane. *Sci. Adv.* **2020**, *6*, eabb5898. [CrossRef] [PubMed]
32. Das, S.; Chen, H.Y.; Penumatcha, A.V.; Appenzeller, J. High performance multilayer $MoS_2$ transistors with scandium contacts. *Nano Lett.* **2013**, *13*, 100–105. [CrossRef] [PubMed]
33. Zheng, X.; Calò, A.; Albisetti, E.; Liu, X.; Alharbi, A.; Arefe, G.; Liu, X.; Spieser, M.; Yoo, W.; Taniguchi, T.; et al. Patterning metal contacts on monolayer $MoS_2$ with vanishing Schottky barriers using thermal nanolithography. *Nat. Electron.* **2019**, *2*, 17–25. [CrossRef]
34. Buscema, M.; Island, J.O.; Groenendijk, D.J.; Blanter, S.I.; Steele, G.A.; van der Zant, H.S.; Castellanos-Gomez, A. Photocurrent generation with two-dimensional van der Waals semiconductors. *Chem. Soc. Rev.* **2015**, *44*, 3691–3718. [CrossRef] [PubMed]
35. Butt, N.Z.; Sarker, B.K.; Chen, Y.P.; Alam, M. Substrate-induced photofield effect in graphene phototransistors. *IEEE Trans. Electron Devices* **2015**, *62*, 3734–3741. [CrossRef]
36. Fang, H.; Hu, W. Photogating in low dimensional photodetectors. *Adv. Sci.* **2017**, *4*, 1700323. [CrossRef]
37. Kim, S.; Maassen, J.; Lee, J.; Kim, S.M.; Han, G.; Kwon, J.; Hong, S.; Park, J.; Liu, N.; Park, Y.C.; et al. Interstitial Mo-assisted photovoltaic effect in multilayer $MoSe_2$ phototransistors. *Adv. Mater.* **2018**, *30*, 1705542. [CrossRef]
38. Lan, Z.; Lei, Y.; Chan WK, E.; Chen, S.; Luo, D.; Zhu, F. Near-infrared and visible light dual-mode organic photodetectors. *Sci. Adv.* **2020**, *6*, eaaw8065. [CrossRef]
39. Lopez-Sanchez, O.; Lembke, D.; Kayci, M.; Radenovic, A.; Kis, A. Ultrasensitive photodetectors based on monolayer $MoS_2$. *Nat. Nanotechnol.* **2013**, *8*, 497–501. [CrossRef]
40. Gao, J.; Zhang, B.; Nie, K.; Xu, J. Research on a pulse-based high-line-rate TDI CMOS image sensor. *Microelectron. J.* **2021**, *111*, 105021. [CrossRef]
41. Zhang, X.; Fan, W.; Xi, J.; He, L.; Hu, C. 14-Bit Fully Differential SAR ADC with PGA Used in Readout Circuit of CMOS Image Sensor. *J. Sens.* **2021**, *2021*, 6651642. [CrossRef] [PubMed]
42. Yu, H.; Liao, M.; Zhao, W.; Liu, G.; Zhou, X.J.; Wei, Z.; Xu, X.; Liu, K.; Hu, Z.; Deng, K.; et al. Wafer-Scale Growth and Transfer of Highly-Oriented Monolayer $MoS_2$ Continuous Films. *ACS Nano* **2017**, *11*, 12001–12007. [CrossRef] [PubMed]